RECONSTRUCTION OF SWEEP MRI SIGNALS

By

Tegan Emerson, Yu Sun, Robert Alvarez, Fataneh Esteki, Huong Le, and Steen Moeller

IMA Preprint Series #2430

(August 2014)

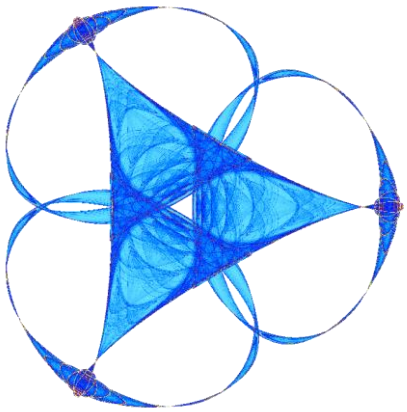

INSTITUTE FOR MATHEMATICS AND ITS APPLICATIONS
UNIVERSITY OF MINNESOTA
400 Lind Hall
207 Church Street S.E.
Minneapolis, Minnesota 55455-0436
Phone: 612-624-6066 Fax: 612-626-7370
URL: http://www.ima.umn.edu

Reconstruction of Sweep MRI Signals

Tegan Emerson[1], Yu Sun[2], Robert Alvarez[3], Fataneh Esteki[4], Huong Le[5], and Steen Moeller[6]

[1] *Colorado State University*
[2] *University of Delaware*
[3] *Arizona State University*
[4] *University of Calgary*
[5] *University of Toronto*
[6] *University of Minnesota Twin Cities*

August 18, 2013

Abstract

In this research, we evaluate two methods of Sweep MRI signal reconstruction to aid in improvement of 3D images generated from Sweep MRI data. A background section has been provided to establish context for our problem statement. Next, we derive the Sweep MRI signal equation which has some convenient properties that will be exploited in our reconstruction methods. We simulate perfect Sweep MRI signal by convolving the radio frequency (RF) and the Free Induction Decay (FID) to obtain a baseline for comparison of the methods. From there we generate authentic Sweep MRI signals where we have zeroed out components of the RF pulse to simulate the switching on and off of the RF pulse. Following the generation of authentic signal, we remove components of the signal to represent the reality of Sweep MRI. Given these realistic Sweep MRI signals with missing data, we reconstruct the FIDs using two methods. First, we use deconvolution to determine the FID. For our second reconstruction method we derived how to apply a method which was previously published specifically for reconstruction of standard MRI signals. We refer to the original method as the Kuethe algorithm, and we refer to our modified version as Modified Kuethe. In both reconstruction methods we utilize the truncated singular value decomposition to generate pseudoinverse operators. Reconstructed signals are then used to generate 3D images using a provided gridding algorithm. An analysis of the results strongly suggest that the Modified Kuethe algorithm yields improved quality in both the individual signal reconstructions and the quality of the 3D images over deconvolution. Results presented show a level of reconstruction accuracy that has not been previously shown, especially in scenarios which emulate clinical settings.

Keywords:
Sweep MRI, MRI, Truncated Singular Value Decomposition, Convolution, Gridding, Signal Reconstruction

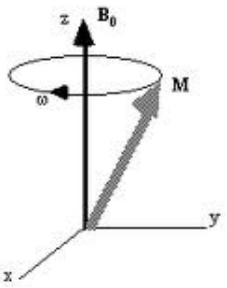

Figure 1: This figure shows the x,y,z-axis M, and there relationship to B_0 [REF]

1 Technical/Biological Background

1.1 Magnetic Resonance Imaging

Magnetic resonance imaging (MRI) is a medical imaging technique used to visualize internal structures of the body in detail. An MRI scanner is a device in which the patient lies within a large, powerful magnet where the magnetic field is used to align the magnetic moment of protons in the body. The scenario in which the magnetic moments are aligned is called the equilibrium state. Next, gradient magnetic fields are applied to alter the alignment of this magnetization[8]. Application of a gradient causes a change in the resonant frequency of protons at different spatial locations. We apply a radio frequencies to excite the protons: higher radio frequency will excite the protons with higher resonant frequency and lower radio frequency will excite the protons with lower resonant frequency. When the radio frequency pulse ends, the protons will go back to the equilibrium state. This causes the protons to produce a rotating magnetic field detectable by the scanner–and this information is recorded to construct an image of the scanned area of the body[9]. By using gradients in different directions, 2D images or 3D volumes can be obtained in any arbitrary orientation.

1.2 Spatial Encoding for MRI

The time-based generated signal detected in the receiver coil caused by oscillating transverse component of magnetization, is called FID. An FID decays over time exponentially. In fact as net magnetization returns to equilibrium, the amplitude of the FID gets smaller over time. The magnitude of the FID depends on the flip angle, the equilibrium value of the magnetization vector, and the strength of the applied magnetic field. The frequency of the FID signal is proportional to the magnitude of magnetic field gradient. We define the coordinate system as Figure 1.

In general we use the set of FIDs to process and reconstruct our images [10], and [6].

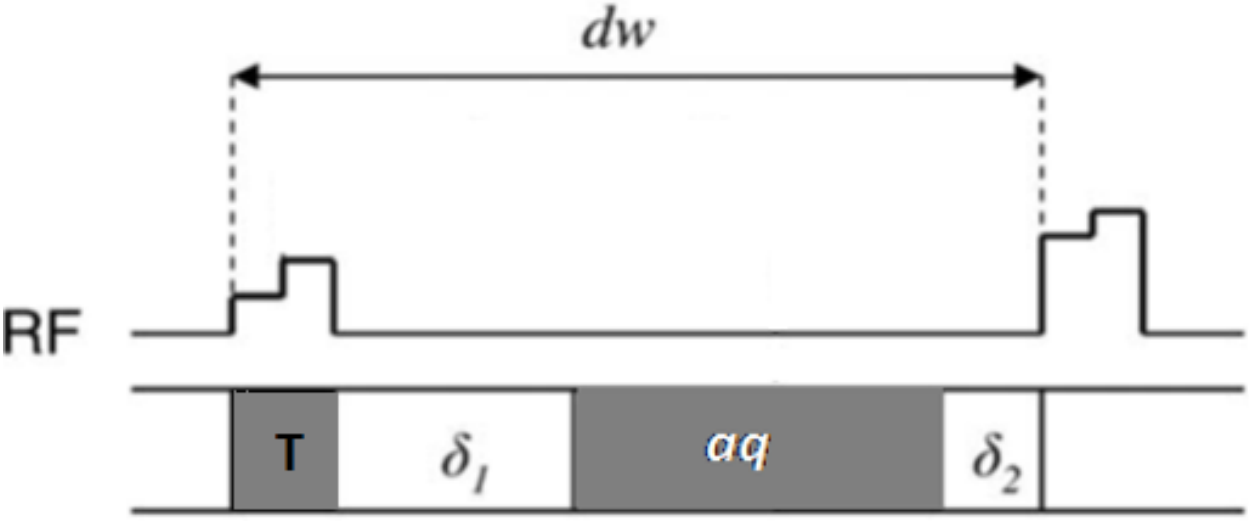

Figure 2: This figure shows the details of one sampling interval during RF sweep [REF].

1.3 Sweep Magnetic Resonance Imaging

MRI is difficult to perform in some body organs that have short lived signals due to fast transverse relaxation or de-phasing. Sweep MRI is a medical imaging modality that attempts to have simultaneous signal acquisition with RF excitation. In reality, sweep MRI implementation relies on interrupting the RF pulses periodically for brief acquisition intervals aq. Hence sweep MRI is still subject to the time to play out an RF pulse T, the time to switch from RF transmission to signal reception δ_1 and the time to switch from signal reception to RF transmission δ_2. As a consequence of the RF pulse durations and machine switching times, data acquisition starts after a net dead time $\Delta = T + \delta_1$ after each time the RF pulse is turned on and off. Thus, both the initial part of the FID is missed, along with periodically missing data until the RF pulse application has been ceased. Two other important parameters of sweep MRI are the projection's bandwidth bw and the signal sampling interval dw which will be referred to as the dwell time. In order to understand these two parameters bw and dw, we recall that we use a magnetic gradient field to make the magnetic environment different at different points in space so that we can get a different response to a given time dependent RF-field. The projections of an object are band-limited due to the finite size of any object being scanned. We denote the bandwidth of our projection to be bw. The signal sample interval dw is the time interval during which we are required to acquire at least one sampling data point to satisfy the Nyquist criterion.

1.3.1 Fourier Transform

A Fourier transform (FT) transforms allows one to move between a function occurring a time domain to the same function represented in the frequency domain. In both Sweep MRI and standard MRI the data acquired corresponds to induced current measurements in the receiver coil over time. However, in order to generate our image we seek to define the projection. Our projection corresponds to a density function representing the number of protons excited at a given frequency. Thus, the projection exists in a frequency domain. The consequence of this relationship between the FID and the projection is that in order to move from the FID to the projection all we must do is compute a Fourier transform and perform a transformation of our projection to ensure that it is zero frequency centered. We can then conclude that if provided with a perfect FID then we can construct the projection using a FT. Additionally, given that we acquire data at a discrete number of even spaced points we are able to move between an FID and a projection using the discrete Fourier transformation.

1.3.2 Derivation of the Sweep MRI Signal Equation

Here we try to derive the equation of signal that allows us to describe the basic principles of MRI.

The signal equation can be derived by solving the Bloch Equation.

In general, the behavior of magnetization vector M is describe by Bloch equation:

$$\frac{dM}{dt} = M \times \gamma B - \frac{M_x i + M_y j}{T_2} - \frac{(M_z - M_0)k}{T_1},$$

where M_0 is equilibrium magnetization, γ ia a constant, B includes the various magnetic field applied, and T_1 is the time constant characterizing the return of magnitization vector along the z-axis and T_2 is the time constant characterizing the decay of the vector component in the xy plane.

Assuming T_1 and T_2 are infinite and imploying Bloch Equation we observe that

$$\frac{dM_x}{dt} = \gamma M_y B_z(t),$$
$$\frac{dM_y}{dt} = -\gamma M_x B_z(t),$$
$$\frac{dM_z}{dt} = 0.$$

We define $M_{xy} = M_x + iM_y$. Hence

$$\frac{dM_{xy}}{dt} = -i\gamma M_{xy} B_z(t) = -iM_{xy}(\gamma r G(t)),$$

$$-\ln M_{xy} = \int i\gamma r G(t) dt + C.$$

This implies

$$M_{xy}(r,t) = exp\left(\int_{\tau}^{t} i\gamma r G(t')dt' + C\right) = M_{xy_0}(r)exp\left(\int_{\tau}^{t} i\gamma r G(t')dt'\right),$$

where $M_{xy}(r,t)$is the evolution function for spin at r.

Therefore the total impulse function is

$$M_{xy}(t) = \int M_{xy}(r,t)dr.$$

Suppose ϕ is a linear system operator, and $p(t)$ is input or RF pulse, which could be represented by the following form:

$$p(t) = \int_{\infty}^{\infty} p(\tau)\delta(t-\tau)d\tau$$

Then our signal $s(t)$ could be represented as:

$$s(t) = \phi(p(t)) = \int_{\infty}^{\infty} p(\tau)\phi(\delta(t-\tau))d\tau$$

Let $h(t,\tau) = \phi\{\delta(t-\tau)\} = M_{xy}(t)$, Then

$$h(t,\tau) = \int M_{xy_0} exp\left(\int_{\tau}^{t} i\gamma r G(t')dt'\right) dr.$$

Define $G(t) = G_0 g(t)$, $\omega = \gamma r G_0$ and $M_{xy_0}(\omega) = H(\omega)M_0 sin(\theta)$. then

$$h(t,\tau) = A_1 \int_{-\infty}^{\infty} H(\omega) exp\left(i\omega \int_{\tau}^{t} g(t')dt'\right) d\omega,$$

where A_1 is a constant.

So the signal equation can be written as

$$\begin{aligned} s(t) &= \int_{-\infty}^{\infty} p(\tau)h(t,\tau)d\tau \\ &= \int_{-\infty}^{\infty} p(t-\tau)h(t,t-\tau)d\tau \\ &= A_1 \int_{0}^{\infty} p(t-\tau)\left\{\int_{-\infty}^{\infty} H(\omega)exp\left(i\omega\int_{t-\tau}^{t} g(t')dt'\right)d\omega\right\}d\tau. \end{aligned}$$

For Signal Equation in discrete time and the gradient G is constant, the Signal Equation can be expressed by

$$s_m = \sum_{l} p_l \int_{V} exp\left\{i\gamma(t_m - \tau_l)G.r\right\}\rho(r)dV,$$

where p_l represents the RF pulse, G denotes the constant gradient vector, $\rho(r)$ is the longitudinal magnetization, where longitudinal magnetization is the magnetization vector along z-axis.

To retrieve the spin density $H(\omega)$ we use a special transform to obtain:

$$S(\omega') = \int_{-\infty}^{\infty} s(t) e^{-i\omega' \int_0^t g(t')dt'} g(t)dt.$$

Note that in our case $g(t)$ is a constant. Hence

$$\begin{aligned} S(\omega') = A \int_{-\infty}^{\infty} \left\{ \int_0^{\infty} p(t-\tau) \int_{-\infty}^{\infty} H(\omega) e^{i\omega f(t)} e^{-i\omega f(t-\tau)} d\omega d\tau \right\} e^{-i\omega' f(t)} g(t)dt = \\ A \int_{-\infty}^{\infty} \int_{-\infty}^{\infty} \left\{ \int_0^{\infty} p(t-\tau) exp(-i\omega f(t-\tau)) d\tau \right\} H(\omega) e^{i\omega f(t)} e^{-i\omega' f(t)} g(t) d\omega dt. \end{aligned} \tag{1}$$

Let $X(\omega) = \int_0^{\infty} p(t) exp(-i\omega \int_0^t g(t')dt')dt$. Since

$$\int_{-\infty}^{\infty} exp(i(\omega - \omega')f(t))g(t)dt = \int_{-\infty}^{\infty} exp(i(\omega - \omega')f)df = 2\pi\delta(\omega - \omega'),$$

we see that

$$S(\omega') = 2\pi A \int_{-\infty}^{\infty} X(\omega) H(\omega) \delta(\omega - \omega') d\omega.$$

Merge the constant into spin density we have

$$S(\omega') = X(\omega')H(\omega'),$$

The above shows that by applying inverse Fourier transform we are able to write the signal equation in terms of convolution of RF and FID.

$$s = RF * FID$$

The derivations of the Sweep MRI signal equation is a reproduction of the derivations shown in [12] and [6].

2 Technical/Computational Background

2.1 Concepts

2.1.1 Nyquist Sampling

In order to get a good reconstruction from our data, we need to make sure we are sampling enough times so that we are not prone to aliasing errors. One theorem that gives concrete results about how many samples are needed per acquisition is given by the Nyquist Sampling Theorem [7]. A simplified form of the theorem can be stated as follows:

> If a function $x(t)$ contains no frequencies higher than B hertz, it is completely determined by giving its ordinates at a series of points spaced $1/(2B)$ seconds apart. [5]

In other words, a function that is bandlimited can be reconstructed from a countable sequence of samples if the number of samples is greater than twice the bandwidth. If this criteria is not met, the reconstruction if prone to aliasing errors and the resulting image will not be representative of the actual image [11]. To formalize this, let $f_s = 1/T$ be the sample rate (in samples per second) and B be the bandwidth. A sufficient condition for reconstruction to reconstruct the original signal from its samples is $f_s > 2B$. This condition is called the Nyquist Criterion [5].

2.1.2 Truncated Singular Value Decomposition and Convolution

The sweep imaging with Fourier transform (SWIFT) signal S' can be viewed as a convolution of the input RF pulse and the FID. An advantage of the convolution is that it is a linear operation and hence can be written as a product of a matrix EE and the FID.

$$S' = RF * FID = EE \cdot FID \tag{2}$$

where $EE \in R^{(mxn)}$ is a rectangular matrix with $m \geq n$. The singular value decomposition (SVD) of EE is

$$EE = U \cdot \Sigma \cdot V' = \sum_{i=1}^{n} u_i \sigma_i v_i' \tag{3}$$

where $U = (u_1, \ldots, u_n)$ and $V = (v_1, \ldots, v_n)$ are matrices with orthonormal columns and where $\Sigma = diag(\sigma_1, \ldots, \sigma_n)$ is a diagonal matrix of singular values of EE that decrease along the diagonal:

$$\sigma_1 \geq \sigma_2 \geq \ldots \sigma_n \geq 0 \tag{4}$$

Since sweep MRI faces data missing problem, the matrix EE is often ill-conditioning. That is as the dimensions of EE get bigger, the more singular values σ_i get smaller, causing the solutions FID change drastically. In order to get the FID, the deconvolution is done via Pseudo inverse which is computed using algorithm based on truncated SVD (TSVD). TSVD of EE is obtained by truncating the SVD expansion of EE at desired threshold ϵ.

$$EE_T = U \cdot \Sigma_T \cdot V^T == U \cdot \begin{bmatrix} \begin{bmatrix} \sigma_1 & & \\ & \ddots & \\ & & \sigma_k \end{bmatrix} & \\ & \end{bmatrix} \cdot V^T \tag{5}$$

where $\sigma_1/\sigma_k \leq \epsilon$ and $\sigma_1/\sigma_{k+1} > \epsilon$. The FID immediately follows by Pseudo inversion,

$$FID = EE_T^+ \cdot S' = V \cdot \begin{bmatrix} \begin{bmatrix} \frac{1}{\sigma_1} & & \\ & \ddots & \\ & & \frac{1}{\sigma_k} \end{bmatrix} & \\ & \end{bmatrix} \cdot U^T \cdot S' \tag{6}$$

Then image reconstruction is done by taking Fourier transform (FT) of the FID.

2.2 Reconstruction Methods

2.2.1 Deconvolution

Since the Sweep MRI signal could be written as the convolution of the RF pulse and the FID.

$$S = RF * FID \tag{7}$$

where S represents the Sweep MRI signal. We could generate a matrix E to represent the convolution with RF in the sense that

$$RF * FID = E \times FID \tag{8}$$

To mimic the actual facts, we drop some data in S. Then we will delete the corresponding rows of E to get a new matrix EE, such that

$$S' = EE \times FID \tag{9}$$

Where S' is the Sweep MRI signal with missing data. Then we could solve the equation (9) with the method of TSVD to get our FID.

2.2.2 Kuethe and Modified Kuethe Method

Dean Kuethe *et al* present three methods for signal reconstruction with missing data in [4]. Although there are three different methods described in [4], the authors spend a great deal of time proving the equivalence of the methods under certain conditions.The setup of their problem is based on current MRI methodology. However, due to some characteristics of the current MRI implementation, there are frequently points missing at the beginning of the acquired signal (the FID). Missing points at the beginning of acquisition can result in a high level of image deterioration, which can affect a radiologist's interpretation of images, and consequently the patient. We are therefore strongly motivated to reconstruct the missing data in an accurate fashion. Kuethe *et al* suggest to perform a reconstruction exploiting two crucial assumptions. First, it is assumed that we know the locations of the missing data. Second, the object is assumed to be band limited. We will begin by describing the method we have chosen to modify. Next, we will discuss each of the two assumptions necessary for the method and how they are applied to our Sweep MRI scenario.

Let us define s to be the signal acquired from an MRI with data acquisition done after the termination of the radio frequency pulse. We will assume that s is discrete and contains N observations. The first assumption of the paper we take into consideration is that we know the locations of our missing data. Thus, we can construct a modified signal d that only includes the truly known values of the signal. To this end we build an $N \times N$ matrix C which is diagonal satisfying $C_{n,n} = 1$ if the n^{th} component of s is known, and zero otherwise. This yields $d = Cs$. Next, we recall that the echo, s, is the Fourier transformation of the

projection, x. Consequently, we can write $s = Fx$, where F is the discrete Fourier transformation matrix of appropriate size. Additionally, we implement the second assumption that the object is band limited by zeroing out components of the projection that we know should be zero due to being outside the bandwidth. Our implementation of this second assumption is done by stating that $x = Tx$ where T is an $N \times N$ diagonal matrix satisfying $T_{n,n} = 1$ only if we know that the n^{th} frequency is within the bandwidth. Pulling all of these assumptions and equalities together produces the statement

$$d = CFTx.$$

We can then solve directly for our projection by using the truncated singular value decomposition methods previously discussed.

Sweep MRI is different in a few significant ways from the MRI methodology assumed by Kuethe. First, the data missing in Sweep MRI is not localized to just the beginning of the acquired signal. The pattern of known versus unknown signal points repeats on finite time intervals. A consequence of this is that our C matrix is more sparse that the C presented in [4]. Second, the signal we obtain is the convolution of our radio frequency pulse and the FID, as shown by the derivation of the Sweep MRI signal equation. This means that in order to draw parallels between the Kuethe method and ours we must first deconvolve our signal to obtain our FID. Additionally, since deconvolution yields the FID and not the echo, we only have F_+x, the Fourier transform of the positive frequencies of the projection after the projection has been shifted to center the density of the $\omega = 0$ frequency. From this we note an issue of dimensions. Our input signal, the deconvolved Sweep MRI signal, $\hat{s}$, will have length M and the projection, x, will have length $2M$. Following the ideology of the Kuethe paper we are thus motivated to define $\hat{C}$ such that $\hat{C}_{m,m} = 1$ if the m_{th} component of the Sweep MRI is known. If we assume a limited bandwidth of the object, we then define T to be the matrix, such that they add zeros equally on both sides of the projection that correspond to the locations we know will have no proton density.

$$x = Tx \tag{10}$$

We recall that the projection is zero frequency centered which means we need to account for this shift. We can account for the shift by appropriately shifting T, and represents it as T'. Then we do a Fourier Transform to the projection we will obtain the echo where time equals zero corresponds to the middle of the echo. Here we also need to do a shift, which we also could act on the matrix F, and represent by F'. Then we get the echo with the peak in the middle. Then we cut the matrix F'T' by half, only leave the lower part on the matrix, we represent it as $\hat{FT}_+$, so that we could get the FID.

Finally, this culminates in our formulation of the Kuethe problem:

$$\hat{C}\hat{s} = \hat{C}\hat{FT}_+x$$

This final formulation of our problem can also be solved using truncated singular value decomposition. All results discussed have been generated by deconvolving the Sweep MRI signal to obtain $\hat{s}$ and then solving the presented system.

2.2.3 Gridding

The Fourier transform has been used extensively throughout our work in Sweep MRI. The biggest issue with the inverse problem for reconstructing our images is that the data for our FIDs must lie on a cartesian grid. In practice, this is not feasible, *e.g.* hardware constraints, practical applications, etc., so we must adopt new methods to reconstruct our data appropriately. The original algorithm we use was developed by Jackson *et al.* [3], where the data samples are weighted for sampling density and convolved with a finite kernel, then resampled on a grid preparatory to a fast Fourier transfom [3]. The modification we make to the gridding algorithm is by using the density correction function developed by Bydder *et al* [1] instead of the original one in [3]. The algorithm we use from [3] is as follows:

Consider a two-dimensional function $m(x, y)$ with Fourier transform $M(u, v)$ given by

$$M(u,v) = \int_{-\infty}^{\infty} m(x,y) e^{-2\pi i(ux+vy)}\, dxdy$$

and a sampling function S consisting of two-dimensional delta functions at positions u_j, v_j,

$$S(u,v) = \sum_{j=1}^{P} \delta^2(u-u_j, v-v_j)$$

The sampled Fourier data is given by

$$M_S(u,v) = M(u,v) \cdot S(u,v)$$

The sampled data is then convolved with a Keiser-Bessel function, $K(u, v)$, and sampled onto a unit spaced grid,

$$M_{SCS}(u,v) = [M_S(u,v) * K(u,v)] \cdot \Pi(u,v) = \{[M \cdot S] * K\} \cdot \Pi$$

where $*$ denotes two-dimensional convolution, and the Π function, $\Pi(u, v)$, is defined as a sum of equally spaced two-dimensional delta functions:

$$\Pi(u,v) = \sum_i \sum_j \delta^2(u-i, v-j)$$

The corresponding reconstructed image, m_{SCS} is given by the inverse Fourier transform of M_{SCS},

$$m_{SCS}(x,y) = \{[m(x,y) * s(x,y)] \cdot k(x,y)\} * \Pi(x,y)$$

The inverse Fourier transform of the original sampling function, $S(u, v)$, which we refer to as $s(x, y)$, affects the aliasing of $m(x, y)$ at a level that cannot be recovered. Thus, as expected, if the function $M(u, v)$ is not sufficiently sampled, the aliasing cannot be corrected via postprocessing. We can, however, make a correction for non-uniform sampling density in $S(u, v)$, by introducing an area density function, $\rho(u, v)$. In our work, we use the area density function by Bydder *et al* [1]. As discussed in the work by Jackson *et al* [3], the

principal transfer (PTF) is given by $S(u,v)/\rho(u,v)$. Introducing the area density function into the reconstruction above, we generate the sampled, weighted, convolved, and sampled M,

$$M_{SWCS}(u,v) = \left\{ \left[\frac{M_S(u,v)}{\rho(u,v)} \right] * K(u,v) \right\} \cdot \Pi(u,v) = \left(\left\{ M \cdot \left[\frac{S}{S * K} \right] \right\} * K \right) \cdot \Pi$$

The corresponding image is given by

$$m_{SWCS}(x,y) = \left(\left\{ m(x,y) * \left[s *^{-1} (s \cdot c) \right] \right\} \cdot c \right) * \Pi,$$

where $*^{-1}$ refers to a deconvolution.

3 Results

Our goal in this section is to present a set of reconstructions of FIDs which highlight the benefit of using our modified implementation of the method described in [4]. We will first present a quantitative analysis of the improvement in reconstruction using our modified Kuethe method as we vary different parameter values. Next, we will show select pictures that qualitatively illustrate our marked improvement in reconstruction that has been quantitatively described. These two analysis are done based on reconstructing a single FID. After we have presented the results on a single FID, we will demonstrate the consequence of using this reconstruction on the generation of a 3D image.

Moving forward, it serves us to define several terms and abbreviations that will be seen frequently in the following analysis.

3.1 Parameter Definitions

- **True FID (TF)**refers to the FID that would be obtained assuming simultaneous radio frequency transmission and data acquisition.
- **Sweep MRI FID (SMF)** refers to the FID that is obtained by deconvolving the Sweep MRI signal. This deconvolution requires the correct modification of the radio frequency pulse to account for when the pulse is on or off.
- **Modified Kuethe FID (MKF)** refers to the reconstructed FID obtained by feeding the "Sweep MRI FID" into our modified Kuethe algorithm.
- **OSR** is the over-sampling rate. Equivalently, this is the number of points which could be acquired in one unit of time satisfying the Nyquist criterion.
- **DW** is an abbreviation of "Dwell Time." The dwell time is the duration of time in which one data point needs to be acquired in order to satisfy the Nyquist criterion.
- δ**DW** refers to the length of time corresponding to **dw** being divided into the number of subcomponents equal to the OSR.

- **T** is the number of δ**DW**s the RF pulse is turned on.
- δ_1 is the number of δ**DW**s that it takes for the machine to switch from transmission of the RF pulse to acquisition of signal.
- **AQ** is the number of δ**DW**s during which data is acquired.
- δ_2 is the number of δ**DW**s required for the machine to switch from receiving signal to transmitting the RF pulse again.

All results shown assume that $\mathbf{T}+\delta_1+\mathbf{AQ}$=2DW (16 δ**DW**) and δ_2=0, unless otherwise indicated. We have chosen to have $\mathbf{T}+\delta_1+\mathbf{AQ}$=2DW to represent a scenario that stands somewhere between an unrealistic time frame and the time frame truly necessary for clinical application. A final assumption that we make is that over a full cycle of **T**, δ_1, and **AQ** we miss only the first $.5\times\mathbf{T}+\delta_1$ data points. This value has been phenomenologically defined.

3.2 Reconstruction of FIDs

3.2.1 Quantitative

Figure 3 shows plots demonstrating the relative error of the Modified Kuethe FID (MKF) and Sweep MRI FID (SMF) as we vary **T** and δ_1. In Figures 3 (a) and 3 (b) we compute the relative error using a weighted 2-norm. Our weight vector w is defined such that $w_i = 1$ if we have confidence that the point was properly acquired and $w_i = 0$ if we believe the point to be incorrectly acquired. The classification of "properly" acquired versus "incorrectly" acquired is based directly on our assumption that we miss only the first $.5\mathbf{T}+\delta_1$ data points. Figures 3 (c) and 3 (d), however, show plots of the relative error of MKF and SMF, respectively, where we compute the relative error using a standard 2-norm. Here the relative error takes into consideration all data points, regardless of our believed accuracy of acquisition. We see illustrated in Figure 3 that whether we use only the points we believe to be accurately acquired or all of the reconstructed data, MKF has a lower relative error that SMF in almost all cases. While the difference in relative error is far more pronounced in the case where all data points are included, the improvement is still nontrivial in the case of only accurate points. The exceptions where SMF has a lower relative error than MKF occur for $\mathbf{T}$=2,4 with high values of δ_1. In interpreting this result it is important to recall that we assume the number of points missing per cycle is computed by $.5\mathbf{T}+\delta_1$. Significance of these observations will follow in the Discussion portion.

3.2.2 Qualitative

Since relative error can be strongly influenced by just a few points being significantly off from truth, we have chosen to highlight what changes of relative error look like by comparing the TF, the Sweep SMF, and the MKF visually. First, in Figure 4 we show how each of the three FIDs look when $\mathbf{T}$=2 but δ_1 is varied. Figures 4(a)-(c) correspond to δ_1=0,6,12 respectively. An important observation we see highlighted in this figure is the lowering of the left most

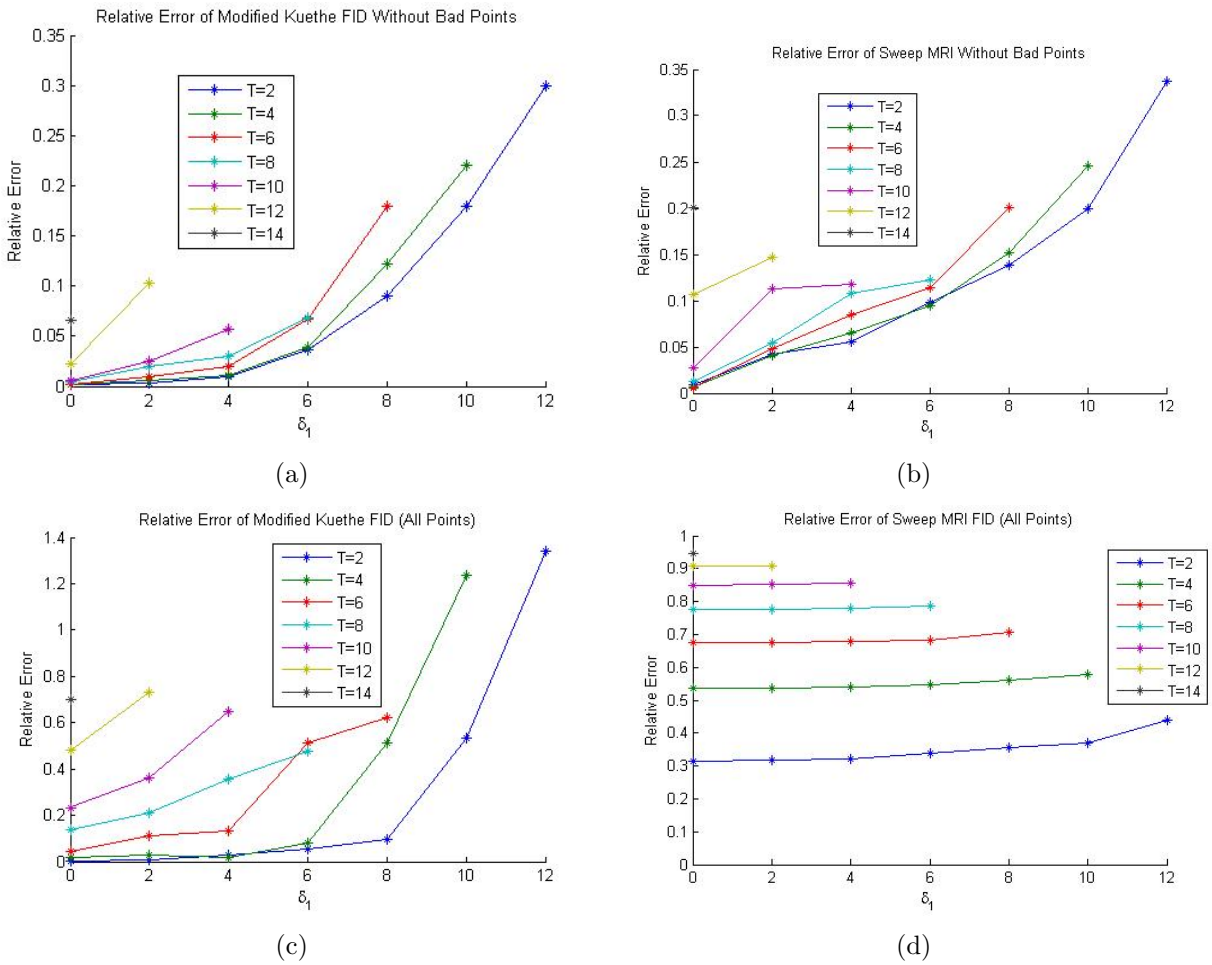

Figure 3: (a)-(b) Show the relative errors of the modified Kuethe FID and Sweep MRI FID, respectively, where the relative error is computed using a weighted norm which ignores all points which we assume to be "bad" based on their corresponding location in the acquired signal. (c)-(d) Show the relative errors of the modified Kuethe FID and Sweep MRI FID, respectively, where the relative error is computed accounting for all data points including the ones we know are "bad."

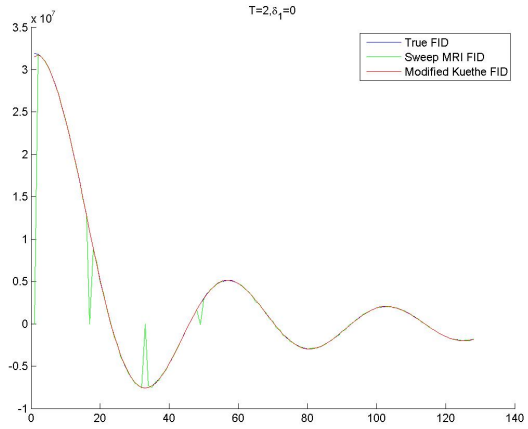

(a)

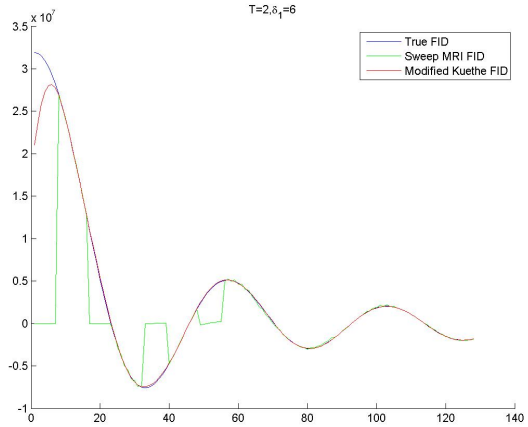

(b)

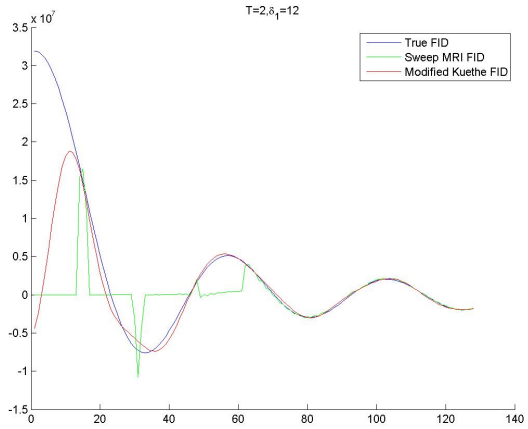

(c)

Figure 4: This figure shows how the two different reconstructions compare for a fixed value **T**=2, as we vary δ_1. In (a) δ_1=0, (b) δ_1=6, and in (c) δ_1=12.

end of MKF as we increase δ_1. The MKF matches the TF more readily over the course of the entire FID than SMF, but the increase in relative error as δ_1 is increased can be largely attributed to the growing distance between the TF and MKF over the first several points. Additionally, when evaluating these pictures we note that we are visually only comparing the first 128 time observations. We do this because of the length of the radio frequency we have used in all of the experiments, since once the pulse is off, we assume all of our gathered points will be accurate. Furthermore, as we continue observing figures, it is pertinent to note that once $.5\times\mathbf{T}+\delta_1 \geq 8$, we have missed data from a full **DW** and expect to see less accurate reconstructions. Missing a full **DW** worth of data later on in the signal is a less damaging, but in our context we start by missing a full **DW**, and then continue to miss full **DW**s later on in the signal, too.

The purpose of Figure 5 is to illustrate weaker impact in changes of **T** compared to changes in δ_1. Figure 5 (a) shows reconstructions for **T**=2, and δ_1=2, while Figure 5 (b) shows reconstructions for **T**=, and δ_1=2. The difference between Figure 4(a) and Figure 4(b) is a 6δ**DW** increase in δ_1. We can readily perceive the change in the quality of the reconstructions in these figures. However, when we fix δ_1=2, and change **T** by 6δ**DW** there is a less apparent change in the reconstructions.

Thus far we have shown reconstructions built on a **T**, δ_1, **AQ** cycle occurring within a 2**DW** time frame. This time frame, however, is not realistic. In reality machines will have a $\delta_1 \geq$1**DW**. For this reason we chose to try to implement our reconstruction method with a **T**, δ_1, **AQ** cycle taking 3**DW**. Particularly, we have chosen **T**=8, δ_1=8, and **AQ**=8, which is equivalent to 1**DW** for each component of the cycle. In Figure 6 we can see the result of the reconstructions under the previously mentioned conditions. This reconstruction is perhaps our most significant contribution from this exploration as it is one of the first times a strong FID reconstruction has been generated in a scenario that may actually be implementable by clinical machinery.

3.3 Gridding Using Reconstructed FIDs

We have just discussed the performance of our reconstruction method applied to reconstructing a single FID. Our goal, however, is to have a clinical impact. In clinical settings it is not a single FID that is observed, but rather a 3D image generated using thousands of FIDs. Thus, in order to later discuss the significance of our findings we need to explore the quality of 3D image generated using our reconstructed FIDs. To this end, we have chose to use MKF and SMF to reconstruct 4,096 FIDs which we then fed into our gridding algorithm. Figure 7 contains a three versions of a single slice of a 3D image generated using our gridding algorithm. All three subfigures were generated using 4,096 FIDs. What differentiates the subfigures is the how the FIDs are obtained. For Figure 7(a) we provided the gridding algorithm with TFs, for Figure 7(b) we provided the gridding algorithm with SMFs, and for Figure 7(c) we provided the gridding algorithm with MKFs. Clearly, the slice generated from our MKFs is over lower quality that the slice from TFs. However, the difference between the slice from MKFs and the slice from SMFs shows a marked improvement in the quality of the images. Generating a 3D image generated from MKFs results in some artifacts in the image,

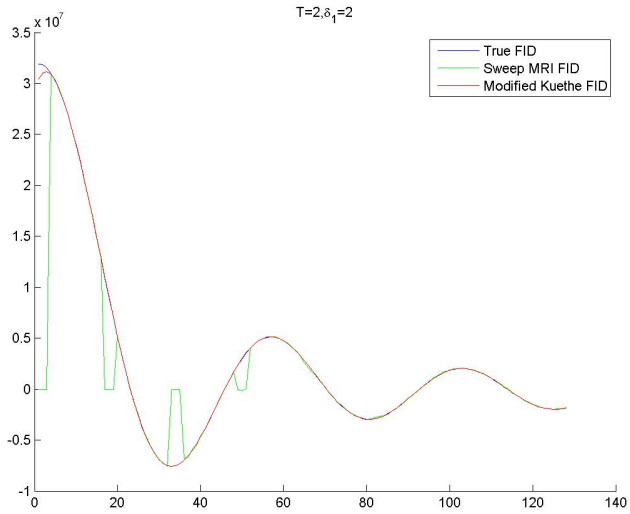

(a)

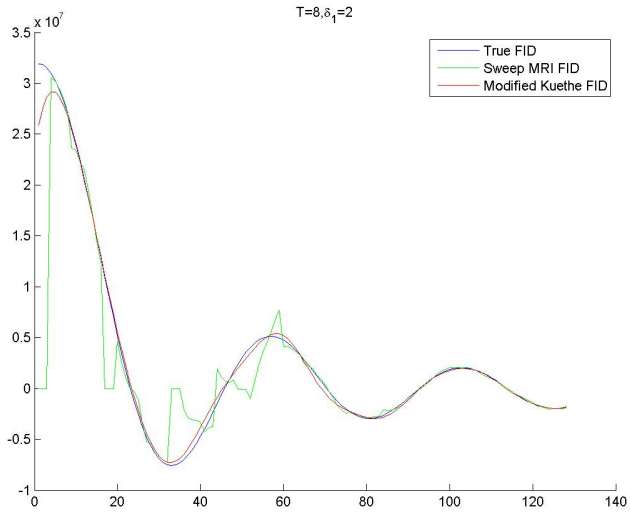

(b)

Figure 5: This figure shows how the two different reconstructions compare for a fixed value δ_1=2, as we vary **T**. In (a) **T**=4 while in (b) we have **T**=8.

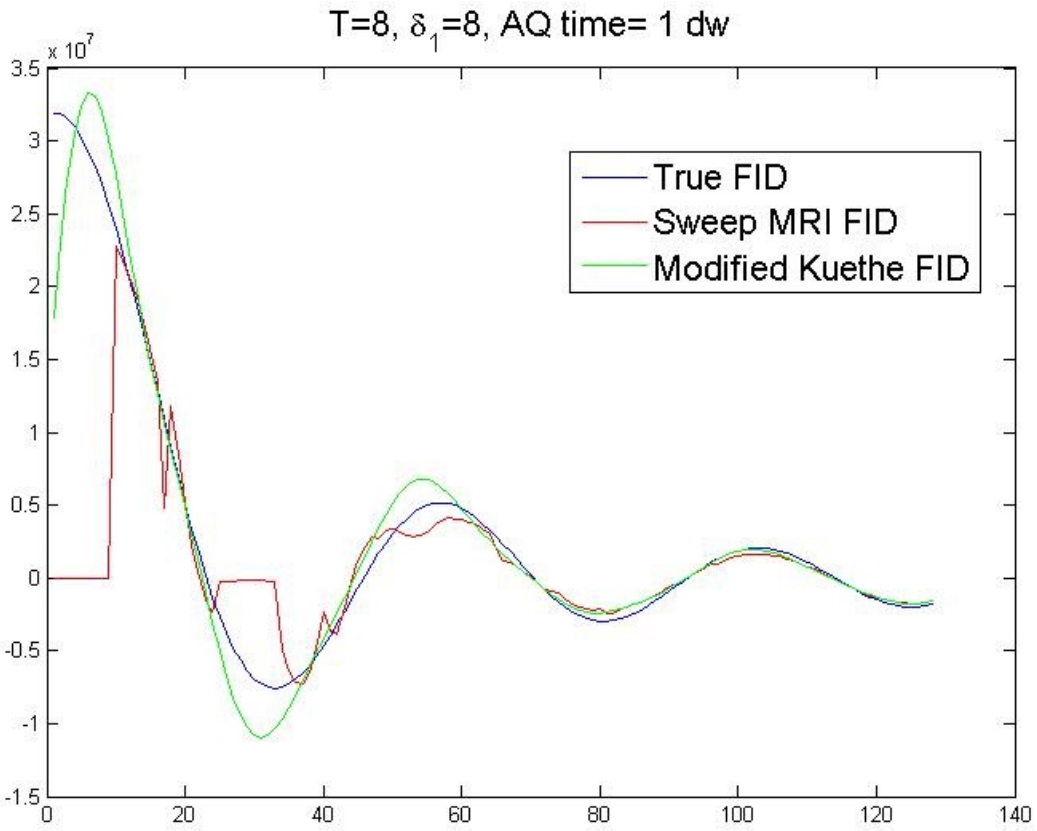

Figure 6: This figure shows how the two different reconstructions compare when a **T**, δ_1, **AQ** cycle takes 3**DW**. We have set **T**=8, δ_1=8, and **AQ**=8.

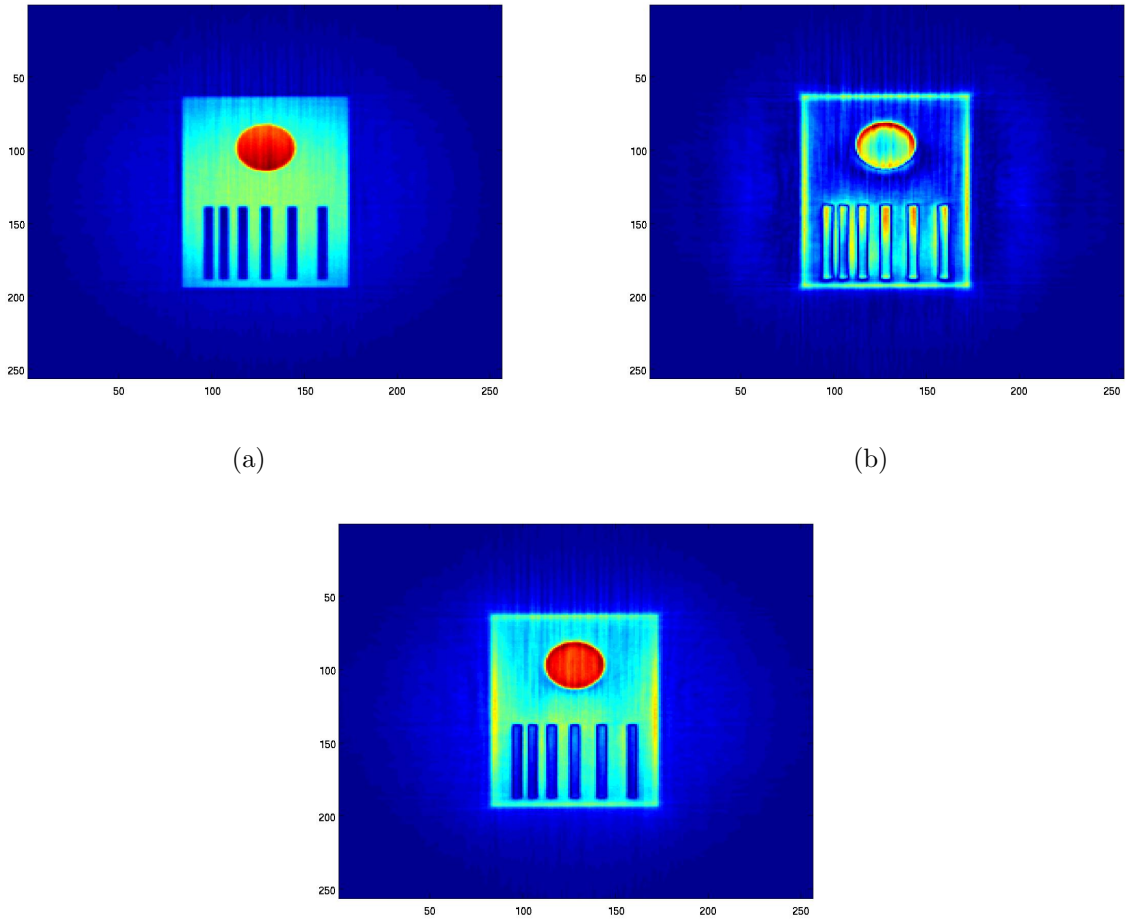

(a)

(b)

(c)

Figure 7: This figure shows a single slice of a 3D image generated in three different fashions. (a) Is the a slice taken from a 3D image generated using 4,096 TFs. (b) Shows the same slice as (a) but where the 3D image is generated using 4,096 SMFs. Lastly, (c) contains the same slice generated from 4,096 MKFs.

but the edges are notably sharper and the interior more consistently filled than the images generated from SMFs. This is strictly a qualitative analysis. A next step in evaluation of our results would be to have a radiologist evaluate the 3D images generated using the different FIDs on a real data set for diagnostic purposes.

4 Discussion

4.1 Observations and Clinical Relevance

The results presented in the previous section allows for several observations to be made. First, both the quantitative and qualitative analysis strongly suggest that the modified Kuethe reconstruction methods will yield higher quality reconstructions than the deconvolution method. This result in and of itself inspires hope that Sweep MRI may find its way into clinics sooner rather than later. In particular, our ability to reconstruct and FID with high levels of accuracy when we simulate a $\mathbf{T}$, δ_1, $\mathbf{AQ}$ cycle taking place over three dwell times. Our ability to reconstruct well where we do not begin to acquire data for two dwell times means that machines in clinical settings may be able to implement Sweep MRI.

While all the results indicate promise, there are some components that are still unclear. First, we do not understand the exact relationship between the number of points that can truly be missing before our reconstruction is no longer close enough (by some undisclosed measure) to the true FID in the first stretch of time. It does not appear to be that it happens exactly after one dwell time worth of data has been skipped. From inspection it appears that there is a ratio of how many sub-dwell times are used for acquisition over the number of sub-dwell times that are missed. However, it is unclear exactly what the ratio must be. Additionally, it was surprising to see such strong reconstruction where the $\mathbf{T}$, δ_1, $\mathbf{AQ}$ cycle took place over three dwell times while there were some reconstructions for a two dwell time cycle which looked farther off. We hypothesize that this is connected to the unknown ratio.

In order to evaluate the clinical relevance we need to understand the best measure of our success. Is success a quantitative measure or a qualitative measure? Are images that are satisfactory to a radiologist for diagnostic purposes good enough, even if by numerical means the difference seems significant? These are questions that we cannot yet answer, but would aim to explore in our future work.

4.2 Future Work

In addition to defining the appropriate measures of success for clinical implementation, there are many other results we would like to explore. To start, we would like to understand the unknown ratio that accounts for some of our more surprising results by exploring more combinations of time for our $\mathbf{T}$, δ_1, $\mathbf{AQ}$ cycles. Next, we would like to explore the role δ_2 plays in results. Additionally, we would like to validate the phenomenologically defined number of points we can assume to be bad given a particular $\mathbf{T}$ and δ_1, and also evaluate how δ_2 changes this number. Also, in both of our reconstruction methods we use truncated

singular value decomposition (TSVD) to determine a pseudoinverse. A threshold parameter is used in TSVD and we have done no optimization of this particular parameter.

5 Disclosures

We would like to clearly state that all results presented here in are the results of preliminary research and cannot be considered conclusive at this juncture. The code used to generate these results will be evaluated and modified to account for any inaccuracies before any results will be published. Additionally, we would like to disclose that there was different authorship of different sections. Not all information presented may be completely accurate, but rather as accurate as the knowledge of the material of each individual author allowed. Each author should be considered independently and only held accountable for the material they have contributed. Finally, we would like to acknowledge that although we never directly site the article many of the ideas surrounding Sweep MRI were first presented in [2].

6 References

References

[1] Mark Bydder, Alexey A Samsonov, and Jiang Du. Evaluation of optimal density weighting for regridding. *Magnetic resonance imaging*, 25(5):695–702, 2007.

[2] Djaudat Idiyatulli, Curt Corum, Jang-Yeon Park, and Michael Garwood. Fast and quiet mri using a swept radiofrequency. *Journal of Magnetic Resonance*, 181:342–349, 2006.

[3] John I Jackson, Craig H Meyer, Dwight G Nishimura, and Albert Macovski. Selection of a convolution function for fourier inversion using gridding [computerised tomography application]. *Medical Imaging, IEEE Transactions on*, 10(3):473–478, 1991.

[4] D. O. Kuethe, A. Caprihan, I. J. Lowe, D. P. Madio, and H. M. Gach. Transforming NMR Data Despite Missing Points. *Journal of Magnetic Resonance*, 139:18–25, July 1999.

[5] II Marks and J Robert. *Introduction to Shannon sampling and interpolation theory*. Springer-Verlag New York, Inc., 1991.

[6] G. Nishimura. *Magnetic Resonance Imaging*. 1996.

[7] Harry Nyquist. Certain topics in telegraph transmission theory. *American Institute of Electrical Engineers, Transactions of the*, 47(2):617–644, 1928.

[8] W.C. Sheil. Magnetic resonance imaging (mri scan). *MedicineNet.com*, 27 April 2012.

[9] Squire LF and Novelline RA. *Squire's fundamentals of radiology (5th ed.)*. ISBN 0-674-83339-2. Harvard University Press, 1997.

[10] unknown. Free induction decay. `http://www.merriam-webster.com/medical/free\%20induction\%20decay/`. Accessed: 2013-08-15.

[11] unknown. Nyquist sampling. Wikipedia. Accessed: 2013-08-15.

[12] unknown. Theory and simulation. Steen Moeller.